Biophysical Journal Volume 102 April 2012 1570–1579

pH-Responsive Titratable Inotropic Performance of Histidine-Modified Cardiac Troponin I

Nathan J. Palpant,[†*] Evelyne M. Houang,[†‡] Yuk Y. Sham,[‡] and Joseph M. Metzger[†*]
[†]Department of Integrative Biology and Physiology, University of Minnesota Medical School; and [‡]Center for Drug Design, University of Minnesota Academic Health Center, Minneapolis, Minnesota

ABSTRACT Cardiac troponin I (cTnI) functions as the molecular switch of the thin filament. Studies have shown that a histidine button engineered into cTnI (cTnI A164H) specifically enhances inotropic function in the context of numerous pathophysiological challenges. To gain mechanistic insight into the basis of this finding, we analyzed histidine ionization states in vitro by studying the myofilament biophysics of amino acid substitutions that act as constitutive chemical mimetics of altered histidine ionization. We also assessed the role of histidine-modified cTnI in silico by means of molecular dynamics simulations. A functional in vitro analysis of myocytes at baseline (pH 7.4) indicated similar cellular contractile function and myofilament calcium sensitivity between myocytes expressing wild-type (WT) cTnI and cTnI A164H, whereas the A164R variant showed increased myofilament calcium sensitivity. Under acidic conditions, compared with WT myocytes, the myocytes expressing cTnI A164H maintained a contractile performance similar to that observed for the constitutively protonated cTnI A164R variant. Molecular dynamics simulations showed similar intermolecular atomic contacts between the WT and the deprotonated cTnI A164H variant. In contrast, simulations of protonated cTnI A164H showed various potential structural configurations, one of which included a salt bridge between His-164 of cTnI and Glu-19 of cTnC. This salt bridge was recapitulated in simulations of the cTnI A164R variant. These data suggest that differential histidine ionization may be necessary for cTnI A164H to act as a molecular sensor capable of modulating sarcomere performance in response to changes in the cytosolic milieu.

INTRODUCTION

Cardiac contraction and relaxation occur through cyclic interactions of the thin and thick filaments of the sarcomere (1). The key allosteric regulatory complex that mediates the transition between the systolic and diastolic phases of the cardiac cycle is troponin (2,3). Troponin is a heterotrimeric protein complex that comprises three subunits: the tropomyosin-binding subunit, troponin T (TnT); the calcium-binding subunit, troponin C (TnC); and the actomyosin ATPase inhibitory subunit, troponin I (TnI) (4,5). After excitation of cardiac muscle, calcium release from the sarcoplasmic reticulum binds to the N-terminal region of TnC. Allosteric changes in cardiac TnC (cTnC) cause the switch arm of TnI to develop an affinity for TnC measured as an increase of two orders of magnitude (6). This increased affinity causes a translocation of the entire regulatory arm of TnI (residues 138–210) and binding of TnI with the N-terminal hydrophobic patch of TnC by multiple van der Waals contacts (7,8). Binding of TnI to TnC during systole causes an allosteric opening of the hydrophobic patch of TnC (6). During diastole, calcium is resequestered into the sarcoplasmic reticulum, causing its dissociation from TnC. TnI subsequently releases TnC and binds actin at both the inhibitory region and the C-terminal region (9–11). This initiates diastole by inhibiting actin-myosin cross-bridge formation. With this important role of TnI differentially toggling between actin and TnC, and thus regulating cross-bridge cycling events, TnI has come to be known as the molecular switch of the myofilament (12).

Studies using acutely isolated adult rat myocytes showed that myofilament sensitivity to activating calcium (pCa) is markedly diminished during acidosis (13). These reports indicate that the pCa ($-\log[Ca^{2+}]$) required for 50% activation of myofilaments in acutely isolated adult cardiac myocytes drops during acidification (from pH 7.0 to 6.2) (13). These experiments illustrate that myofilament Ca^{2+} desensitization at low pH is a fundamental molecular deficiency that underlies, in part, myocyte and cardiac organ pathologies associated with myocardial acidosis (14).

Recent studies showed that a unique histidine moiety in the regulatory arm of TnI (slow skeletal TnI (ssTnI) H132 and cardiac TnI (cTnI) A164H) acts as a pH-dependent titratable inotrope that is capable of ameliorating contractile deficiencies caused by acidosis in vitro (13,15) and in vivo (15–17) (Fig. 1). Here, a cognate histidine button, when engineered into cTnI, functions as a molecular sensor with no significant contractile effects at baseline but marked enhancement of inotropic performance under various pathophysiological stresses, including acute and chronic myocardial ischemia and acidosis (15–18).

The histidine-button switch mechanism plays a critical role in mediating several biological functions by altering intra- and intermolecular structures and interactions. For example, this molecular switch role for histidine is observed

Submitted July 20, 2011, and accepted for publication January 17, 2012.

*Correspondence: metzgerj@umn.edu or npalpant@uw.edu

Nathan J. Palpant's present address is Center for Cardiovascular Biology and Regenerative Medicine, University of Washington Medical School, Seattle, WA.

Editor: Malcolm Irving.

0006-3495/12/04/1570/10 $2.00

doi: 10.1016/j.bpj.2012.01.024

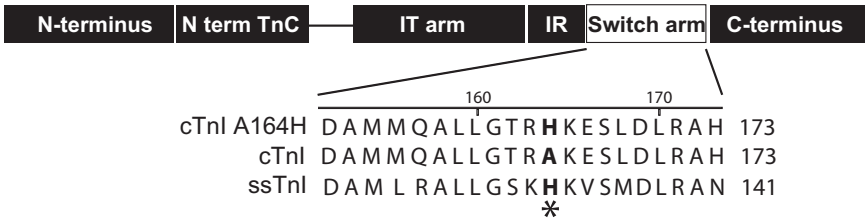

FIGURE 1 Primary amino-acid sequence of cTnI A164H, WT cTnI, and ssTnI within the TnI regulatory switch arm.

in hemoglobin, where H146β mediates the Bohr effect by altering its pH-dependent intramolecular interaction with D94β (19,20). In addition to TnI and hemoglobin, numerous other histidine buttons in biology have been identified, including HLA-DR molecules (21), GABA ρ1 receptors (22), the pacemaker channel HCN2 (H321) (23), the acid-sensitive potassium channel TASK-3 (H98) (24), the inward rectifying potassium channel HIR (H117) (25), and the G-protein-coupled inward rectifying potassium channel (GIRK1/GIRK4)(H64, H228, and H352) (26).

Histidine is unique among amino acids in that its chemical nature and pH-responsive binary ionization states enable it to mediate the switch function of pH-responsive buttons in the physiological pH range. The differential ionization of histidine within the physiologic range is principally due to its unique imidazole side chain, which has a pKa of ~6.0. The nonprotonated histidine is hydrophobic and aromatic in character, whereas the protonated histidine is hydrophilic and positively charged.

The implications of a histidine modification for cTnI structure and function are not well understood. Investigators have employed numerous strategies involving site-directed mutagenesis to analyze the molecular mechanism of histidine buttons in other molecules (19–21,24,25).

In this work, our main goal was to gain mechanistic insight into the function of cTnI. To that end, we analyzed cellular contractile performance to understand the functional implications of arginine (cTnI A164R) as a biochemical mimic of the protonated histidine compared with the contractile dynamics of wild-type (WT) cTnI (A164) and cTnI A164H. To further elucidate the structural dynamics of the His-164 moiety in cTnI, we used molecular dynamics (MD) simulations to examine the structural dynamics in the calcium-saturated cTn complex. This study provides the first evidence, to our knowledge, that differential imidazole side-chain ionization is the molecular basis for the titratable, inotropic performance of histidine-modified cTnI.

METHODS

cTnI in situ protein mutagenesis and viral vector construction

We used a pDC315 adenoviral shuttle vector containing cTnI and the QuikChange mutagenesis kit (Stratagene) to generate site-directed mutagenesis. As previously described (15), the primers used for mutagenesis of cTnI to cTnIA164H FLAG removed an Xma1 site and were 5′- ggcactactggggacccggcacaaggaatccttggacctg-3′ (sense) and 5′-caggtccaa ggattccttgtgccgggtccccagtagtgcc-3′ (antisense). Mutagenesis of cTnI A164R FLAG was generated from the cTnI A164H FLAG cDNA. Primers used for mutagenesis from cTnI A164H FLAG to cTnI A164R FLAG were 5′- gcactactggggacccggcgcaaggaatccttgg-3′ (sense) and 5′- ccaaggatt ccttgcgccgggtccccagtagtgc -3′ (antisense). In all cases, the primers were extended with Pfu DNA polymerase, and methylated parental DNA was subsequently digested with Dpn I. DNA was transformed into competent bacterial cells. Mutated DNA with appropriate restriction enzyme sites was sequenced before the mutant cTnI cDNA was ligated into Ad5 viral shuttle vectors. All DNA sequences were verified by overlapping sequence runs. The cTnI FLAG vector was produced and used as previously described (27), and used here as a control for viral transduction and the FLAG epitope. Recombinant vectors were produced and purified as described previously (28).

Ventricular myocyte isolation, gene transfer, and primary culture

Adult rat ventricular myocytes were isolated as previously described (17,29,30). Briefly, adult female rats were anesthetized by inhalation of isoflurane followed by i.p. injection of heparin (1500 U/kg) and Nembutal (162.5 U/kg). Following enzymatic digestion by retrograde perfusion with collagenase and hyaluronidase, and gentle mincing of the cardiac ventricles, the cardiac myocytes were plated on laminin-coated glass coverslips (2×10^4 myocytes/coverslip) and cultured in M199 media (Sigma, St. Louis, MO) supplemented with 10 mmol/L glutathione, 26.2 mmol/L sodium bicarbonate, 0.02% bovine serum albumin, and 50 U/ml penicillin-streptomycin, with pH adjusted to 7.4, as described previously (31). Recombinant adenovirus was applied to the cells immediately after plating, as previously described (29). The cells were subsequently cultured for 4 days to provide sufficient time for stoichiometric replacement of TnI proteins delivered by adenoviral gene transfer.

Immunoblot detection

The myocytes were removed from coverslips and placed in Laemmli sample buffer. Proteins were separated by SDS-PAGE and transferred to a nitrocellulose membrane for immunodetection. After blocking in 5% milk (in Tris-buffered saline), membranes were probed with a pan TnI antibody (MAB1691; Chemicon, Billerica, MA). Indirect immunodetection was carried out using a fluorescently labeled secondary antibody (IRDye 680 conjugated affinity purified, 1:5000; Rockland, Gilbertsville, PA). Western blot analysis was performed on an infrared imaging system (Odyssey; Li-Cor, Milton, MA), and images were analyzed with Odyssey software v. 1.2.

Indirect detection of incorporation by immunofluorescence and confocal microscopy

Dual-labeling immunofluorescence was performed as previously described (12). Briefly, cultured cardiac myocytes were fixed in 3% paraformaldehyde/phosphate-buffered saline and blocked in 20% normal goat serum. Myocytes were incubated in the first primary antibody directed against

the Flag epitope (M2, 1:500; Sigma) and detected with an Alexa 488-conjugated secondary antibody directed against mouse IgG (1:100; Molecular Probes). Myocytes were incubated in the second primary antibody directed against α-actinin (EA53, 1:500; Sigma) and detected with Texas Red-conjugated secondary antibody directed against mouse IgG. All antibodies were diluted in 2% normal goat serum + 0.5% Triton X-100/phosphate-buffered saline. Immunofluorescence was visualized on a Zeiss Axioskop LSM 510 laser scanning confocal microscope.

Contractility measurements in single intact myocytes

Sarcomere length (SL) shortening and relaxation kinetics were performed as previously described (17,29). Briefly, coverslips containing single isolated myocytes were placed on an inverted microscope (Eclipse TE2000; Nikon) and stimulated at 0.2 Hz. The chamber's temperature was maintained at 37°C. Myocyte images were collected (240 Hz) with a CCD camera (MyoCam; IonOptix). Myocytes that did not follow the pacing protocol (0.2 Hz) or had a resting SL of <1.70 μm were excluded. SL shortening and relaxation kinetics were calculated with the use of IonOptix software. Myocytes were initially analyzed under baseline conditions in M199 (pH 7.4). To elucidate the changes in myocyte performance during exposure to acidosis, the same myocyte preparations were subsequently incubated with acidic M199 (pH 6.2). In vivo NMR-based tracking of cardiac muscle intracellular pH has shown we are working in the pH range found in ischemic hearts (15). Other investigators (32) and we have used this pH differential to assess the effects of acidosis on cellular biophysics. pH 7.4 mimics physiological pH, whereas pH 6.2 mimics acidosis levels observed in the ischemic heart. Because control (nontransduced) and cTnIFLAG-transduced myocytes had no functional difference in sarcomere contractile kinetics, the data were combined into the control dataset. The summary data for myocyte contractile parameters are outlined in Table S1 of the Supporting Material.

Skinned myocyte tension pCa measurements

Single rod-shaped cardiac myocytes were attached to micropipettes coated in silicone adhesive and permeabilized in 0.2% Triton X-100 for 1 min. All measurements were made at 15°C in relaxation (RS) or activating solutions (AS). Both RS and AS contained 1 mmol/L free Mg^{2+}, 4 mmol/L MgATP, 14.5 mmol/L creatine phosphate, 20 mmol/L imidazole, and potassium chloride to yield an ionic strength of 180 mmol/L. Solution pH was adjusted to 7.00 (or 6.20 for acidic pH experiments) with potassium hydroxide/hydrochloric acid. The pCa ($-\log[Ca^{2+}]$) of the RS was 9.0, and the pCa of maximal AS was 4.0. The SL was set to 2.1 μm and the isometric tension-pCa relation was constructed by measuring the calcium-activated isometric tension at basal (pCa = 9.0), maximal (pCa = 4.0), and various submaximal calcium levels as previously described (15). Every third contraction was taken at maximal pCa to normalize tension values. A nonlinear least-squares fitting algorithm was used to determine the Hill coefficient (n) and pCa_{50}, the calcium concentration at which 50% of maximal tension was produced. Because the control (nontransduced) and cTnIFLAG genetically engineered myocytes showed no functional difference in steady-state isometric tension-Ca^{2+} relationship, the data were combined into the control dataset. The summary data for myocyte tension pCa analysis and Hill coefficients are outlined in Table S2.

Molecular modeling

Molecular modeling was carried out with the use of the Schrödinger (New York, NY) modeling suite package. The study was carried on the truncated cTnI (residues 148–173): cTnC (residues 1–90) modeled complex based on the x-ray crystallographic structures of the full-length human cTnI (9) (PDB: 1J1E) complexed to Ca^{+2}-bound TnC. The cTnI A164H (residues 148–173)/cTnC (residues 1–90) and cTnI A164R (residues 148–173)/cTnC (1–90) mutant complexes were generated by amino acid substitution. The missing hydrogen atoms were added and energy-minimized using the OPLS 2005 force field (33). The imidazole groups of all histidines in the structure were ionized according to the calculated pKa values.

MD simulation

All simulations were carried out using NAMD (29) version 2.6 with the CHARMM27 protein force field (30) and TIP3P water model (34). Each protein complex was solvated in a rectangular box with a 15 Å water buffer from the protein. Na^+ and Cl^- counterions were added at 5 Å from the box boundary to neutralize the total charge of the system. Each system was initialized by a 5000-step conjugate gradient energy minimization with protein heavy atoms restrained at 50 kcal/(mol · $Å^2$). The restraint system was gradually heated from 25 K to 300 K at 25 K increments at every 10 ps interval for 100 ps, followed by a 100 ps equilibration with gradual removal of the heavy atoms restraint at a 10 ps interval under the NVT condition. The final unrestrained equilibration was carried out for 100 ps followed by 40 ns of production simulation at 1 atm and 300 K under the NPT condition. The simulations were carried out under the periodic boundary condition using particle mesh Ewald (35). The SHAKE method (36) was employed to restrain all hydrogen bonds. A 2 fs time step was used with coordinates saved at 1 ps time intervals, resulting in a total of 40,000 configurations for simulation. Five 40-ns simulations were carried out for each of the modeled complexes by random initialization of the starting velocities.

Interatomic distance calculations

All distances were evaluated in angstrom units over the last 10 ns of the simulation run for each of the simulated trajectories. For the cTnI A164HSD and cTnI A164HSP simulations of the cTnI/cTnC complex, the average distance was evaluated between cTnI H164 (NE2) and cTnC E19 (OE2). Distance measurements were also assessed between cTnI A164R (NH2 or NH1) and cTnC E19 (OE2). Distance measurements for the WT structure were taken between cTnI A164 (CB) and cTnC E19 (OE2).

Root mean-square deviations

Cα residues root mean-square deviations (CαRMSDs) were evaluated using the starting PDB structures as reference throughout each of the full 40-ns simulations.

Theoretical pKa calculations

The general continuum electrostatics method, which is widely used to calculate the energetics of proton transfer and its corresponding pK_a within a consistent thermodynamic cycle, is described elsewhere (37,38). Here, the calculations were carried out based on the web-based implementation of the linearize Poisson-Boltzmann implicit solvent model (37) available via H++ server (39) (http://biophysics.cs.vt.edu/H++/). Briefly, the protein pK_a of ionizable residue, pK_a^p, is evaluated by

$$pK_a^p = pK_a^{int} + \Delta pK_a^{charges}, \quad (1)$$

where pK_a^{int} is the intrinsic pK_a of the ionizable residue inside the protein when all other ionizable groups are in their neutral states, and $\Delta pK_a^{charges}$ represents pK_a shifts due to the charge-charge interaction between the indicated titratable group and all other ionized groups in their average ionization states in the protein. This method allows for a straightforward decomposition of the total computed pK_a value as the sum of the effects due to the change in moving the ionized group from water to the polar environment of the protein when all ionizable groups are set to their neutral state (pK_a^{int}) and its interaction with all other ionizable groups ($\Delta pK_a^{charges}$). Thus, the calculated pK_a values can be used to characterize the strength

of electrostatic interactions between neighboring groups in protein. The pK_a^{int} is evaluated as the change in the self-free energy of the indicated ionizable group in its neutral (AH) and ionized (A^-) state from water to the protein, $\Delta\Delta G_{solv}^{w\rightarrow p}$ and is given by

$$pK_a^{int}(AH) = pK_a^{w}(AH) + \frac{1}{2.303\,RT}\Delta\Delta G_{self}^{w\rightarrow p}(AH\rightarrow A^-) \quad (2)$$

Here pK_a^w is the model pK_a of the amino-acid side chain in water. The electrostatic contribution toward the changes in the self-free energy can be described by

$$\Delta\Delta G_{self}^{w\rightarrow p} = \Delta G_{back}^{p} + \Delta\Delta G_{born}^{w\rightarrow p} \quad (3)$$

where ΔG_{back}^{p} is the interaction between the ionized group with the protein permanent dipoles, and $\Delta\Delta G_{born}^{w\rightarrow p}$ is the free energy of desolvation of moving the group from the water to the protein. We obtained the electrostatic contribution to the self-free energy by evaluating the average electrostatic potential based on the numerical solution to the linearized Poisson-Boltzmann equation:

$$\nabla\cdot\varepsilon(r)\nabla\phi(r) - \kappa^2\varepsilon(r)\phi(r) = -4\pi\rho_0(r) \quad (4)$$

where $\varepsilon(r)$ is the distance-dependent dielectric constant, ϕ(r) is the electrostatic potential at point r, $\rho0(r)$ is the permanent charge density of the solute, and κ is the inverse Debye-Hückel salt-screening length.

In this work, the protein was treated as a low-dielectric medium where $\varepsilon_{in} = 40$, and the surrounding solvent was assigned a high-dielectric constant $\varepsilon_{out} = 80$. The choice of a low protein dielectric constant for pK_a calculation was previously discussed (40), and higher dielectric constants did not appreciably affect the predicted values obtained (Table S3). The Debye-Hückel screening parameter κ was used to set the electrostatic screening effects of the salt concentration corresponding to physiological conditions of 0.145 M. The pK_a values shown in Table 1 were derived by calculating the intrinsic pK_a (pK_{int}), which corresponds to the pK_a of the group of interest wherein all of the other titratable amino acids are maintained in the neutral state (38), and the pK_a from two different structures (20 ns and 40 ns) during the time-course of each simulation.

Statistics

All results are expressed as the mean ± standard error (SE). Multigroup comparisons were assessed by one-way analysis of variance (ANOVA) with the Newman-Keuls post-hoc test, with $p < 0.05$ considered statistically different.

RESULTS

Stoichiometric incorporation of TnI into myocytes after adenoviral gene transfer

We used in vitro methods to address the role of ionization in the molecular inotropic behavior of cTnI A164H. To accomplish this, we generated recombinant adenoviruses expressing various TnI proteins that act as chemical mimetics of different histidine ionization states. These included WT cTnI A164 (constitutively deprotonated mimetic), cTnI A164R (constitutively protonated mimetic), and cTnI A164H (pH-dependent ionization). Stoichiometric expression of exogenously delivered myofilament proteins causes dose-dependent competitive replacement of endogenous proteins to achieve synchronous and efficient genetic modification of adult cardiac myocytes (13,15,17,29). In this study, we delivered specific TnI variants by adenoviral gene transfer to assess their functional effects on the performance of TnI myofilaments in intact and permeabilized myocytes. Beginning on day 1, stoichiometric replacement of endogenous cTnI by AdTnI could be detected by Western blot (Fig. 2 *a*). AdTnI stoichiometric replacement increased progressively until day 4 after gene transfer, at which point genetically modified myocytes showed, in all cases, ~80–90% replacement of endogenous cTnI. Laser scanning confocal microscopy using indirect immunofluorescence against the FLAG epitope showed uniform and precise localization of exogenous TnI proteins in the thin filament of the sarcomere (Fig. 2 *b*).

Myocyte sarcomere function at baseline and during exposure to acidosis

Dynamic SL-shortening and relaxation kinetics, as well as the steady-state isometric tension-pCa relationship, were analyzed 4 days after acute adenoviral-mediated gene transfer into isolated single adult rat cardiac myocytes (Fig. 3 *a*, Table S1, and Table S2). Measurements were taken under baseline and acidic conditions. As a measure of contractility, calcium-activated isometric tension (pCa_{50}) and normalized SL shortening were used as markers of cellular inotropic performance in the context of WT and TnI-modified thin filaments. Baseline analysis of SL shortening and pCa_{50} showed that WT and cTnI A164H-modified myofilaments were not different compared with the heightened myofilament calcium sensitivity and cellular contractility observed in myocytes expressing the cTnI A164R variant ($p < 0.05$ versus WT and cTnI A164H; Fig. 3 *b*). When myocytes were exposed to acidic conditions the contractile function and pCa_{50} of cTnI A164H and cTnI A164R were not statistically different compared with a significantly reduced inotropic capacity and reduced myofilament calcium sensitivity observed in WT myocytes ($p < 0.05$ versus cTnI A164H and cTnI A164R; Fig. 3 *c*). The delta change from baseline to acidosis was calculated to determine the net change in inotropy attributable to reduced pH (Fig. 3 *d*). These data showed that only cTnI A164H had pH-dependent titratable inotropy, as indicated by the maintenance of contractile function and improved calcium sensitivity of the myofilaments during the pH shift compared with WT cTnI and cTnI A164R. In contrast, WT cTnI and cTnI A164R were equally affected by acidosis, as shown by a similar decrease in normalized SL shortening and rightward shift of the pCa_{50} during the pH change. These data are consistent with the hypothesis that the arginine variant, which has a basic R group, functions as a constitutive calcium sensitizer. In contrast, alanine in the WT TnI is nontitratable, consistent with the biochemistry of its methyl group. The histidine substitution provides a substrate for differential ionization

TABLE 1 pK_a calculations for MD simulations

	cTnC, cTnI WT				cTnC/cTnI A164R		
	pK_a^{int} ($\varepsilon_{in} = 4$)	$\Delta pK_a^{charges}$ ($\varepsilon_{eff} = 40$)	pK_a^{p}		pK_a^{int} ($\varepsilon_{in} = 4$)	$\Delta pK_a^{charges}$ ($\varepsilon_{eff} = 40$)	pK_a^{p}
cTnC				cTnC			
Asp-2	3.99	−0.54	3.45	Asp-2	4.00	−0.38	3.62
Asp-3	4.24	−0.40	3.84	Asp-3	4.19	−0.33	3.86
Tyr-5	12.97	0.29	13.26	Tyr-5	12.12	0.35	12.47
Lys-6	9.50	2.76	12.26	Lys-6	9.69	2.77	12.45
Glu-10	4.54	−0.12	4.42	Glu-10	4.56	−0.05	4.51
Glu-14	4.35	−0.17	4.18	Glu-14	4.88	−0.36	4.52
Glu-15	4.10	0.07	4.17	Glu-15	4.37	−0.17	4.21
Lys-17	9.89	1.04	10.93	Lys-17	9.92	1.19	11.11
Glu-19	5.01	−0.63	4.37	Glu-19	5.18	−1.45	3.73
Lys-21	9.99	0.93	10.92	Lys-21	10.03	0.81	10.83
Asp-25	4.62	−0.59	4.03	Asp-25	4.30	−0.42	3.89
cTnI WT				cTnI A164R			
Arg-149	9.82	2.43	12.24	Arg-149	10.05	2.28	12.33
Asp-153	3.68	−0.61	3.06	Asp-153	4.30	−0.77	3.53
Arg-163	9.87	1.88	11.76	Arg-163	10.89	1.05	11.94
				Arg-164	9.86	1.56	11.41
Lys-165	10.22	0.41	10.64	Lys-165	10.10	0.43	10.53
Glu-166	4.93	−0.33	4.60	Glu-166	4.91	−0.73	4.18
Asp-169	3.99	−0.92	3.07	Asp-169	4.62	−0.77	3.85
Arg-171	11.71	0.36	12.07	Arg-171	11.50	0.60	12.10
His-173	6.62	0.43	7.06	His-173	6.95	0.14	7.08
cTnC				cTnC			
Asp-2	3.87	−0.29	3.57	Asp-2	3.93	−0.46	3.59
Asp-3	4.05	−0.22	3.83	Asp-3	4.27	−0.48	3.74
Tyr-5	12.59	0.45	13.04	Tyr-5	12.60	0.57	13.36
Lys-6	9.70	3.26	12.96	Lys-6	9.78	2.28	11.85
Glu-10	4.66	−0.28	4.39	Glu-10	4.61	−0.13	4.48
Glu-14	5.67	−1.18	4.48	Glu-14	4.80	−0.47	4.38
Glu-15	4.35	−0.19	4.16	Glu-15	4.25	0.03	4.27
Lys-17	9.85	1.96	11.81	Lys-17	10.02	1.23	11.38
Glu-19	4.16	−1.25	2.92	Glu-19	4.54	−0.13	4.42
Lys-21	9.93	0.62	10.54	Lys-21	10.16	0.77	10.91
Asp-25	4.58	−0.55	4.03	Asp-25	4.49	−0.67	3.86
cTnI A164H				cTnI A164H			
Arg-149	12.22	2.65	14.87	Arg-149	10.36	2.22	12.51
Asp-153	3.84	−0.50	3.34	Asp-153	4.18	−0.32	3.85
Arg-163	10.65	1.20	11.85	Arg-163	10.50	1.48	12.04
Hsp164	5.90	0.50	6.40	His164	6.52	−0.14	6.46
Lys-165	10.07	1.03	11.10	Lys-165	10.11	0.41	10.52
Glu-166	4.42	−0.31	4.11	Glu-166	5.33	−0.84	4.44
Asp-169	4.53	−1.55	2.98	Asp-169	4.65	−0.90	3.82
Arg-171	11.28	0.76	12.04	Arg-171	11.79	0.34	12.19
His-173	6.44	0.44	6.88	His-173	6.74	0.21	6.95

Predicted protein pKa values for all ionizable residues as an average of the 20-ns and 40-ns structures for cTnI A164 (simulations 1–5), cTnI A164R (simulations 1–4), cTnI A164HSP (simulation 5), and cTnI A164H (simulations 1–5).

due to the unique pKa of its imidazole moiety, which is deprotonated under physiological pH but becomes protonated under mildly acidic conditions. These data also indicate that the histidine-substituted troponin modification of the myofilaments alone cannot account entirely for the pH-dependent titratable inotropy. The calcium sensitivity of the myofilaments was affected by the pH change, albeit not to the extent observed with WT cTnI and cTnI A164R. This evident pH-dependent effect was not observed in the intact myocytes, which in the cTnI A164H context retained baseline contractile performance at acidic pH. Further experiments are required to determine the role of calcium regulation or other potential modulators that may be involved in regulating pH-responsive contractile performance in cardiac myocytes.

Simulation and pKa calculations

We performed an MD simulation of the calcium-saturated state of the cTn complex (7) (PDB: 1j1e chains DEF) to

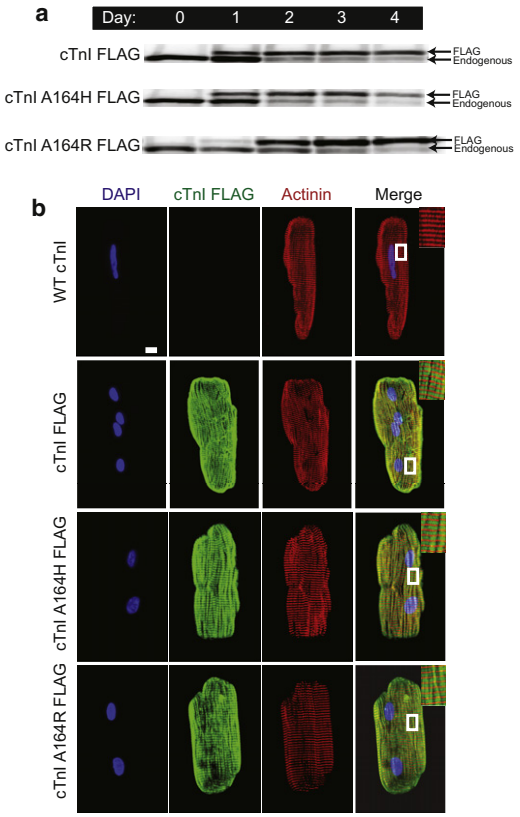

FIGURE 2 Adenoviral gene transfer of TnI into adult rat cardiac myocytes. (*a*) Protein expression by Western blot, showing stoichiometric replacement of endogenous TnI by cTnI FLAG, cTnI A164H, or cTnI A164R over the time course of 4 days of in vitro cell culture. (*b*) Immunofluorescence images showing proper incorporation of cTnI FLAG, cTnI A164H, or cTnI A164R into the thin filament of adult cardiac myocytes after adenoviral gene transfer.

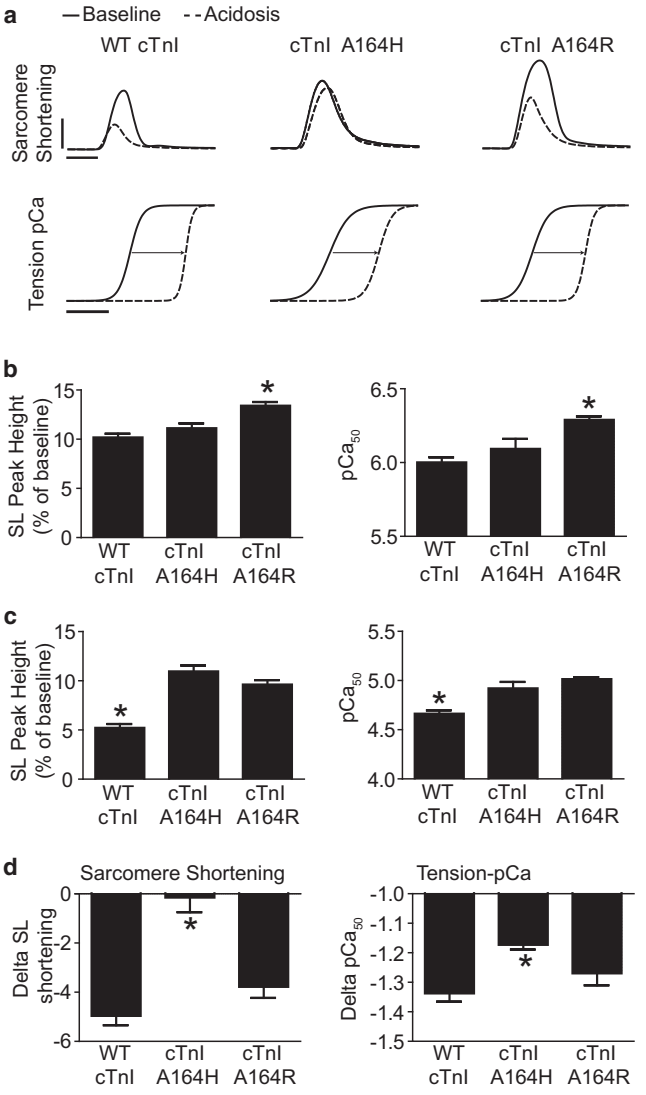

FIGURE 3 SL shortening and tension pCa measurements under physiologic and acidic conditions. (*a*) Top: Raw traces illustrating the change in SL-shortening kinetics between 7.4 and 6.2 for each group (horizontal bar (time) = 0.1 s; vertical bar (SL) = 0.1 μm). Bottom: Normalized tension-pCa_{50} curves illustrating the change in myofilament calcium sensitivity (pCa_{50}) between 7.0 and 6.2 for each group (horizontal bar (pCa_{50}) = 1 U). (*b*) Mean values of percent SL peak height and myofilament pCa_{50} at baseline. (*c*) Mean values of percent SL peak height and myofilament pCa_{50} during exposure to acidosis. (*d*) Mean values showing the δ change from baseline to acidosis in terms of (*left*) SL shortening as a percentage of peak height and (*right*) myofilament pCa_{50}. For all groups, $n > 50$ myocytes from more than three independent myocyte preparations. * $p < 0.05$ compared with all other groups by one-way ANOVA.

gain atomistic insight into the effects of a histidine substitution in cTnI on the intermolecular engagement between cTnI and cTnC. To that end, we performed in silico structural truncation (cTnI (residues 148–173)/cTnC (residues 1–90)) followed by protein mutagenesis (cTnI A164H and cTnI A164R; Fig. 4 *a*).

To assess the effects of the differential ionization states of histidine, we complexed WT cTnC with various TnI structures, including WT cTnI and cTnI A164H (with its imidazole group either deprotonated (cTnI A164HSD) or protonated (cTnI A164HSP)). Similar to in vitro biophysical assays, cTnI A164R was also simulated to determine the effects of a biochemical mimic of protonated cTnI A164H. Atomistic insights into these structural differences were acquired during five independent 40-ns MD simulations of the cTnI/cTnC regulatory engagement in the calcium-saturated state (Movie S1 (simulation 1 for WT cTnI/cTnC), Movie S2 (simulation 1 for cTnI A164HSD/cTnC), Movie S3 (simulation 5 for cTnI A164HSP/cTnC), and Movie S4 (simulation 1 for cTnI A164R/cTnC). Instead of performing a single continuous MD simulation, we carried out multiple short simulations with different starting velocities to assess the potential conformation spaces accessible by the various troponin structures.

To assess the importance of an electrostatic intermolecular contact between position 164 of cTnI and cTnC E19, we obtained interatomic distance measurements across the 40 ns of each structure's MD simulation (Fig. 4, *b*). These data showed no evidence of engagement between cTnC

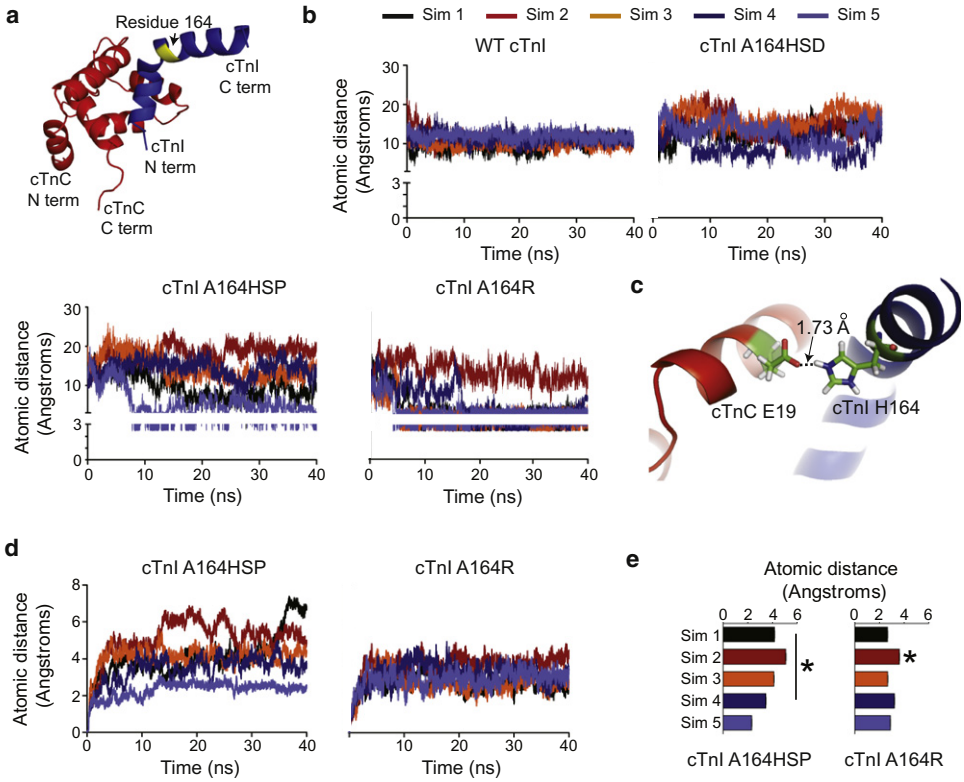

FIGURE 4 MD simulations of the calcium-saturated cTn complex. (*a*) Truncation of the raw crystal structure as reported by Takeda et al. (7) with cTnC residues 1–90 (*red*), and cTnI residues 148–173 (*blue*) used as the starting structure ($t = 0$) for all simulations. The yellow moiety indicates position 164 of cTnI. (*b*) Interatomic distance measurements for all five independent 40-ns simulations of each structure. Distance was measured between cTnC E19 (OE2) and either WT cTnI A164 (CB), cTnI A164HSD (NE2), cTnI A164HSP (NE2), or cTnI A164R (NH2 or NH1). (*c*) Structure of cTnI A164HSP simulation 5 captured at the 40-ns time point, showing a salt bridge between side chains of cTnC E19 and cTnIH164. (*d*) Root mean-square deviation (RMSD) analysis of cTnIA164HSP and cTnIA164R simulations 1–5. (*e*) Average RMSD for each simulation. $^*p < 0.05$ by one-way ANOVA.

E19 and position 164 of WT cTnI (sim 1–5) or cTnI A164HSD (sim 1–5). MD simulations for cTnI A164HSP (sim 1–4) also did not come close enough for salt-bridge formation (Fig. 4 *b*). In contrast, cTnIA164HSP (sim 5) showed structural shifts of helix 4, indicating sustained electrostatic engagement between cTnI H164 and cTnC E19 (Fig. 4, *b* and *c*). Simulations of cTnI A164R, the biochemical correlate of the protonated histidine, showed an even higher probability of salt-bridge formation with cTnC E19 (Fig. 4 *b*). Four out of five MD simulations showed sustained interaction between these two amino acids throughout the experiment. Extraction of a structural snapshot during the MD simulation of the cTnI A164HSP complexed with cTnC shows that cTnI H164 and cTnC E19 interacted to form a salt bridge by hydrogen-bonding at a distance of <3 Å (Fig. 4 *c*).

Root mean-square deviation (RMSD) analysis of all of the cTnIA164HSP MD simulations showed that simulation 5 had the lowest deviation from the starting structure (Fig. 4, *d* and *e*). Beyond the stability of single atomic interactions, these data show evidence of thermodynamic stability across the entire cTnI structure caused, at least in part, by the electrostatic interaction between cTnC E19 and cTnI H164 in the calcium-saturated state. Similarly, structural analysis of the cTnI A164R variant showed that all simulations in which R164 developed a salt bridge with cTnC E19 (simulations 1, 3, 4, and 5) and showed significantly lower RMSDs than the single simulation that failed to form this bond (simulation 2).

Additionally, theoretical side-chain pKa calculations, averaged from multiple simulated structures, showed a marked pK_a^p shift for residues cTnC E19 and cTnI 164 of the A164HSP and A164R structures, consistent with formation of a salt bridge (Table 1). Examination of the A164 and A164H deprotonated simulated structural complexes indicated that residues cTnC E19 and A164H underwent no observable shifts and thus remained solvent-exposed (Table 1).

On the basis of the MD simulation data, a positive charge at cTnI position 164 (either arginine or protonation of histidine's imidazole group) suggests a structural configuration involving a key interaction with cTnC Glu-19. In a comparison of simulated structures, no other major differences were observed in terms of number of intermolecular contacts, average probability of intermolecular atomic interactions, binding energies, and other variables that could account for structure-function correlations due to the histidine substitution (data not shown). Among the variables assessed, the electrostatic interaction between cTnI position 164 (A164HSP or A164R) and cTnC E19 appears to be a unique modifier of structural behavior. Supporting in vitro biophysical assays presented in this study, these data point to a potential mechanism whereby cTnI A164H can maintain inotropy during acidosis.

DISCUSSION

This study provides important insight into the molecular mechanism underlying the pH-responsive titratable

molecular inotropy observed with a single histidine modified cTnI (A164H). Previous reports revealed that a histidine button engineered into the regulatory domain of cTnI provides a substrate for therapeutically modulating cardiac performance in response to various pathophysiological stresses (15–17). However, the molecular mechanism for this phenotype has not been elucidated. In this study, we used in vitro functional analysis and in silico MD simulations to gain insight into the role of differential imidazole ionization in regulating the unique function of histidine-modified cTnI. Theoretical side-chain pKa calculations, averaged from multiple MD simulated structures, provide evidence that the ionization of the imidazole moiety in cTnI A164H is governed primarily by changes in solvent pH, and not by intermolecular electrostatic interactions. Under neutral pH conditions, cTnI A164H has in vitro biophysical properties comparable to those of WT cTnI. Similarly, both WT and cTnI A164H have markedly reduced pCa_{50} and myocyte contractility compared with the constitutively protonated calcium sensitizer cTnI A164R. These data suggest that cTnI A164H remains deprotonated under physiological conditions. Structural simulations further support the hypothesis that deprotonated histidine in cTnI A164H behaves similarly to WT cTnI when complexed with cTnC.

Under acidic conditions, cTnI A164H has in vitro biophysical characteristics of heightened pCa_{50}, and enhanced contractility similar to that of the calcium sensitizer cTnI A164R, the biochemical correlate to a protonated imidazole. This is supported by MD simulations showing that a single proton added to histidine in cTnI A164H may provide a substrate for an electrostatic interaction between H164 of cTnI and E19 of cTnC. However, structural variability is evident in the cTnI A164HSP simulations, suggesting multiple potential structural variations that could give rise to the functional characteristics of cTnI A164H. Structural simulations of cTnI A164R show four of five independent simulations forming a salt bridge between cTnI R164 and cTnC E19. This supports the hypothesis that an electrostatic interaction is structurally favorable within the potential conformational spaces of these proteins when a positive charge is present at cTnI position 164. Together, the in vitro and in silico data support the hypothesis that differential imidazole ionization of histidine enables cTnI A164H to act as a molecular sensor capable of regulating sarcomere function in response to acute and chronic changes to the intracellular biochemical milieu.

Westfall et al. (41) assessed the calcium sensitivity of cardiac myofilaments using chimeric TnI molecules to show a role for the C-terminal region of cTnI in regulating cardiac contractility. Furthermore, Förster resonance energy transfer experiments revealed that movements of the regulatory arm of TnI during systole and diastole are essential for transmitting the calcium signal to the rest of the myofilament proteins (42,43). As a basis for this observation, Li et al. (6) used multinuclear, multidimensional NMR spectroscopy to show that side-chain contacts between the switch peptide of cTnI (residues 147–163) engage the calcium-saturated N-terminal region of cTnC through multiple hydrophobic interactions. This observation was supported by a crystal structure analysis of the calcium-saturated cTn core complex (7). These hydrophobic side-chain contacts were similarly observed in regulatory interactions within the fast skeletal (fs) troponin structure (44).

Gene-transfer and transgenic studies showed that alterations in the peptide composition of the TnI switch arm can markedly alter myofilament performance (15,45–47). Studies with TnI isoform chimeras showed a unique role for the C-terminal domain of ssTnI in modulating myofilament function in response to changes in pH (41,48). Further peptide modifications show a histidine residue in the switch arm as a key moiety responsible for modulating performance in cTnI (cTnI A164H) (15,46). Site directed mutagenesis studies provide evidence that a single histidine to alanine substitution in the switch arm of ssTnI (H132A) causes markedly increased pH sensitivity and a significant diminution in inotropy analogous to WT cTnI (45). Our analysis of the crystal structure of a closely related TnI, fsTnI (44), suggests that H132 engages closely with cTnC E19 in the calcium-saturated state (18). Using MD simulations, we found that an alanine substitution breaks this close intermolecular electrostatic interaction, which is required for heightened inotropy, and eliminates the substrate for pH-responsive histidine ionization, which is necessary for the titratable contractile performance observed with ssTnI (18). Recent findings (18) suggest that cTnC Glu-19 is a critical acidic residue that engages with His-130 of ssTnI (which structurally corresponds to position 164 of cTnI). This electrostatic salt bridge between ssTnI H132 and cTnC E19 appears to be essential for the majority of the binding energy ($\Delta\Delta G$) between these proteins in the calcium-saturated state. In an evolutionary sense, these data suggest that this key residue modification of H132A reduced myofilament calcium sensitivity by making cTnI molecularly untethered from cTnC. We recently proposed that, to meet the demands for refined performance of the mammalian adult heart, compensatory evolutionary pressures favored amino-acid mutations that enhanced the relaxation properties of cTn by decreasing its sensitivity to activating calcium (18). Taking evolution in the reverse direction, the reciprocal substitution in the contemporary milieu of the mammalian cTnI (cTnI A164H) was shown to provide a means of reintroducing pH-responsive titratable contractile performance without enhanced inotropy at baseline (15,16).

This study provides important evidence that histidine imidazole ionization is the primary mechanism for the pH-responsive titratable inotropy observed with cTnI A164H. Under neutral pH conditions, WT cTnI and cTnI A164H behave similarly, based on myofilament sensitivity to pCa and SL-shortening kinetics. The calculated pK_a of

H164 at 6.45 supports a two-state pH-dependent ionizable switch mechanism. We hypothesize that the H164 side chain remains primarily deprotonated under physiological conditions at pH $>$ 7, whereas under acidic conditions at pH $<$ 7, the propensity for H164 imidazole to become protonated will greatly increase. Compared with A164H, the hypercontractility observed with constitutive protonation at residue 164 (cTnI A164R) at baseline supports this conclusion. Thus, at physiological pH, WT cTnI and cTnI A164H have similar molecular inotropic functions mediated by structural dynamics largely involving intermolecular hydrophobic side-chain contacts with cTnC (6,7).

In contrast, under acidic conditions, measures of myofilament sensitivity and SL-shortening dynamics indicate that WT cTnI has significantly compromised inotropic function compared with cTnI A164H and the cTnI A164R variant. The calculated pKa of the A164H side chain indicates that solvent effects on H164 would support imidazole protonation under acidic conditions. As such, the functional implications of histidine ionization are corroborated by MD simulations of cTnI A164H/cTnC and cTnI A164R/cTnC. These simulation data indicate that a protonated moiety in cTnI at position 164 enables cTnI to engage in a more thermodynamically stable conformation with cTnC in the calcium-saturated state, mediated at least in part by an electrostatic contact occurring between cTnI H164 and cTnC E19. Taking the structural, cellular, and organ-level data together, we propose the following model for the titratable inotropy observed with cTnI A164H: solvent-mediated differential ionization of histidine enables cTnI A164H to remain deprotonated at baseline, resulting in inotropy similar to that observed for WT cTnI. As the pH becomes increasingly acidic, protonation of histidine's imidazole group enables the maintenance of baseline myofilament contractile performance, at least in part through this thermodynamically favorable electrostatic contact at the cTnC:cTnI interface.

Understanding the basis for the therapeutic implications of a histidine button in cTnI provides important insights into the mechanisms that modulate cardiac performance in response to ischemia or acidosis. Using cTnI A164H as a gene therapy vector, and identifying small molecules that mimic the pH-responsive features of histidine-modified cTnI may be a valuable approach for treating numerous cardiomyopathies. Specifically, although this molecule has little to no effect on contractile function at baseline, it protects inotropic performance in response to acute or chronic stresses such as myocardial ischemia. The evidence presented here shows that imidazole ionization is necessary for the pH-responsive titratable inotropy observed with myofilaments containing histidine-modified cTnI.

SUPPORTING MATERIAL

Three tables and four movies are available at http://www.biophysj.org/biophysj/supplemental/S0006-3495(12)00097-5.

We thank Lakshmi Mundada for assistance in cloning the expression vectors, and Dr. Brian Thompson for helpful comments on drafts of this work. We also thank the University of Minnesota Supercomputing Institute for providing the computational resources.

This study was supported by the National Institutes of Health (J.M.), the American Heart Association (N.P.), and the University of Minnesota Center for Drug Design (Y.Y.S.).

REFERENCES

1. Gordon, A. M., E. Homsher, and M. Regnier. 2000. Regulation of contraction in striated muscle. *Physiol. Rev.* 80:853–924.
2. Farah, C. S., C. A. Miyamoto, …, F. C. Reinach. 1994. Structural and regulatory functions of the NH2- and COOH-terminal regions of skeletal muscle troponin I. *J. Biol. Chem.* 269:5230–5240.
3. Farah, C. S., and F. C. Reinach. 1995. The troponin complex and regulation of muscle contraction. *FASEB J.* 9:755–767.
4. Greaser, M. L., and J. Gergely. 1971. Reconstitution of troponin activity from three protein components. *J. Biol. Chem.* 246:4226–4233.
5. Filatov, V. L., A. G. Katrukha, …, N. B. Gusev. 1999. Troponin: structure, properties, and mechanism of functioning. *Biochemistry (Mosc.).* 64:969–985.
6. Li, M. X., L. Spyracopoulos, and B. D. Sykes. 1999. Binding of cardiac troponin-I147-163 induces a structural opening in human cardiac troponin-C. *Biochemistry.* 38:8289–8298.
7. Takeda, S., A. Yamashita, …, Y. Maéda. 2003. Structure of the core domain of human cardiac troponin in the Ca(2+)-saturated form. *Nature.* 424:35–41.
8. Dong, W. J., J. M. Robinson, …, H. C. Cheung. 2003. Ca2+-induced conformational transition in the inhibitory and regulatory regions of cardiac troponin I. *J. Biol. Chem.* 278:8686–8692.
9. Brown, L. J., K. L. Sale, …, P. G. Fajer. 2002. Structure of the inhibitory region of troponin by site directed spin labeling electron paramagnetic resonance. *Proc. Natl. Acad. Sci. USA.* 99:12765–12770.
10. Dong, W. J., J. An, …, H. C. Cheung. 2006. Structural transition of the inhibitory region of troponin I within the regulated cardiac thin filament. *Arch. Biochem. Biophys.* 456:135–142.
11. Van Eyk, J. E., and R. S. Hodges. 1988. The biological importance of each amino acid residue of the troponin I inhibitory sequence 104-115 in the interaction with troponin C and tropomyosin-actin. *J. Biol. Chem.* 263:1726–1732.
12. Metzger, J. M., and M. V. Westfall. 2004. Covalent and noncovalent modification of thin filament action: the essential role of troponin in cardiac muscle regulation. *Circ. Res.* 94:146–158.
13. Westfall, M. V., E. M. Rust, and J. M. Metzger. 1997. Slow skeletal troponin I gene transfer, expression, and myofilament incorporation enhances adult cardiac myocyte contractile function. *Proc. Natl. Acad. Sci. USA.* 94:5444–5449.
14. Day, S. M., M. V. Westfall, and J. M. Metzger. 2007. Tuning cardiac performance in ischemic heart disease and failure by modulating myofilament function. *J. Mol. Med.* 85:911–921.
15. Day, S. M., M. V. Westfall, …, J. M. Metzger. 2006. Histidine button engineered into cardiac troponin I protects the ischemic and failing heart. *Nat. Med.* 12:181–189.
16. Palpant, N. J., L. G. D'Alecy, and J. M. Metzger. 2009. Single histidine button in cardiac troponin I sustains heart performance in response to severe hypercapnic respiratory acidosis in vivo. *FASEB J.* 23:1529–1540.
17. Palpant, N. J., S. M. Day, …, J. M. Metzger. 2008. Single histidine-substituted cardiac troponin I confers protection from age-related systolic and diastolic dysfunction. *Cardiovasc. Res.* 80:209–218.
18. Palpant, N. J., E. M. Houang, …, J. M. Metzger. 2010. Pathogenic peptide deviations support a model of adaptive evolution of chordate

cardiac performance by troponin mutations. *Physiol. Genomics.* 42:287–299.

19. Berenbrink, M. 2006. Evolution of vertebrate haemoglobins: histidine side chains, specific buffer value and Bohr effect. *Respir. Physiol. Neurobiol.* 154:165–184.
20. Perutz, M. F., A. M. Gronenborn, …, D. T. Shih. 1985. The pKa values of two histidine residues in human haemoglobin, the Bohr effect, and the dipole moments of alpha-helices. *J. Mol. Biol.* 183:491–498.
21. Rötzschke, O., J. M. Lau, …, J. L. Strominger. 2002. A pH-sensitive histidine residue as control element for ligand release from HLA-DR molecules. *Proc. Natl. Acad. Sci. USA.* 99:16946–16950.
22. Wang, T. L., A. Hackam, …, G. R. Cutting. 1995. A single histidine residue is essential for zinc inhibition of GABA rho 1 receptors. *J. Neurosci.* 15:7684–7691.
23. Zong, X., J. Stieber, …, M. Biel. 2001. A single histidine residue determines the pH sensitivity of the pacemaker channel HCN2. *J. Biol. Chem.* 276:6313–6319.
24. Rajan, S., E. Wischmeyer, …, C. Derst. 2000. TASK-3, a novel tandem pore domain acid-sensitive K^+ channel. An extracellular histiding as pH sensor. *J. Biol. Chem.* 275:16650–16657.
25. Coulter, K. L., F. Périer, …, C. A. Vandenberg. 1995. Identification and molecular localization of a pH-sensing domain for the inward rectifier potassium channel HIR. *Neuron.* 15:1157–1168.
26. Mao, J., J. Wu, …, C. Jiang. 2003. Inhibition of G-protein-coupled inward rectifying K^+ channels by intracellular acidosis. *J. Biol. Chem.* 278:7091–7098.
27. Michele, D. E., F. P. Albayya, and J. M. Metzger. 1999. Thin filament protein dynamics in fully differentiated adult cardiac myocytes: toward a model of sarcomere maintenance. *J. Cell Biol.* 145:1483–1495.
28. Westfall, M. V., E. M. Rust, …, J. M. Metzger. 1997. Adenovirus-mediated myofilament gene transfer into adult cardiac myocytes. *Methods Cell Biol.* 52:307–322.
29. Herron, T. J., R. Vandenboom, …, J. M. Metzger. 2007. Calcium-independent negative inotropy by β-myosin heavy chain gene transfer in cardiac myocytes. *Circ. Res.* 100:1182–1190.
30. Davis, J., H. Wen, …, J. M. Metzger. 2007. Thin filament disinhibition by restrictive cardiomyopathy mutant R193H troponin I induces Ca^{2+}-independent mechanical tone and acute myocyte remodeling. *Circ. Res.* 100:1494–1502.
31. Coutu, P., and J. M. Metzger. 2002. Optimal range for parvalbumin as relaxing agent in adult cardiac myocytes: gene transfer and mathematical modeling. *Biophys. J.* 82:2565–2579.
32. Lee, J. A., and D. G. Allen. 1991. Mechanisms of acute ischemic contractile failure of the heart. Role of intracellular calcium. *J. Clin. Invest.* 88:361–367.
33. Jorgensen, W. L., D. S. Maxwell, and J. Tirado-Rives. 1996. Development and testing of the OPLS all-atom force field on conformational energetics and properties of organic liquids. *J. Am. Chem. Soc.* 118:11225–11236.
34. Jorgensen, W., J. Chandrasekar, …, M. Klein. 1983. Comparison of simple potential functions for simulating liquid water. *J. Chem. Phys.* 79:926–935.
35. Essmann, U., L. Perera, …, L. G. Pedersen. 1995. *J. Chem. Phys.* 103:8577–8593.
36. Ryckaert, J. P., G. Ciccotti, and H. J. C. Berendsen. 1977. *J. Comput. Phys.* 23:327–341.
37. Bashford, D., and M. Karplus. 1990. pKa's of ionizable groups in proteins: atomic detail from a continuum electrostatic model. *Biochemistry.* 29:10219–10225.
38. Sham, Y. Y., Z. T. Chu, and A. Warshel. 1997. Consistent calculations of pK(a)'s of ionizable residues in proteins: semi-microscopic and microscopic approaches. *J. Phys. Chem. B.* 101:4458–4472.
39. Gordon, J. C., J. B. Myers, …, A. Onufriev. 2005. H++: a server for estimating pKas and adding missing hydrogens to macromolecules. *Nucleic Acids Res.* 33(Web Server issue):W368–371.
40. Schutz, C. N., and A. Warshel. 2001. What are the dielectric "constants" of proteins and how to validate electrostatic models? *Proteins.* 44:400–417.
41. Westfall, M. V., F. P. Albayya, …, J. M. Metzger. 2000. Chimera analysis of troponin I domains that influence Ca(2+)-activated myofilament tension in adult cardiac myocytes. *Circ. Res.* 86:470–477.
42. Miki, M., T. Kobayashi, …, Y. Maéda. 1998. Ca^{2+}-induced distance change between points on actin and troponin in skeletal muscle thin filaments estimated by fluorescence energy transfer spectroscopy. *J. Biochem.* 123:324–331.
43. Li, Z., J. Gergely, and T. Tao. 2001. Proximity relationships between residue 117 of rabbit skeletal troponin-I and residues in troponin-C and actin. *Biophys. J.* 81:321–333.
44. Vinogradova, M. V., D. B. Stone, …, R. J. Fletterick. 2005. Ca(2+)-regulated structural changes in troponin. *Proc. Natl. Acad. Sci. USA.* 102:5038–5043.
45. Westfall, M. V., and J. M. Metzger. 2007. Single amino acid substitutions define isoform-specific effects of troponin I on myofilament Ca^{2+} and pH sensitivity. *J. Mol. Cell. Cardiol.* 43:107–118.
46. Dargis, R., J. R. Pearlstone, …, L. B. Smillie. 2002. Single mutation (A162H) in human cardiac troponin I corrects acid pH sensitivity of Ca^{2+}-regulated actomyosin S1 ATPase. *J. Biol. Chem.* 277:34662–34665.
47. Pearlstone, J. R., B. D. Sykes, and L. B. Smillie. 1997. Interactions of structural C and regulatory N domains of troponin C with repeated sequence motifs in troponin I. *Biochemistry.* 36:7601–7606.
48. Westfall, M. V., F. P. Albayya, and J. M. Metzger. 1999. Functional analysis of troponin I regulatory domains in the intact myofilament of adult single cardiac myocytes. *J. Biol. Chem.* 274:22508–22516.